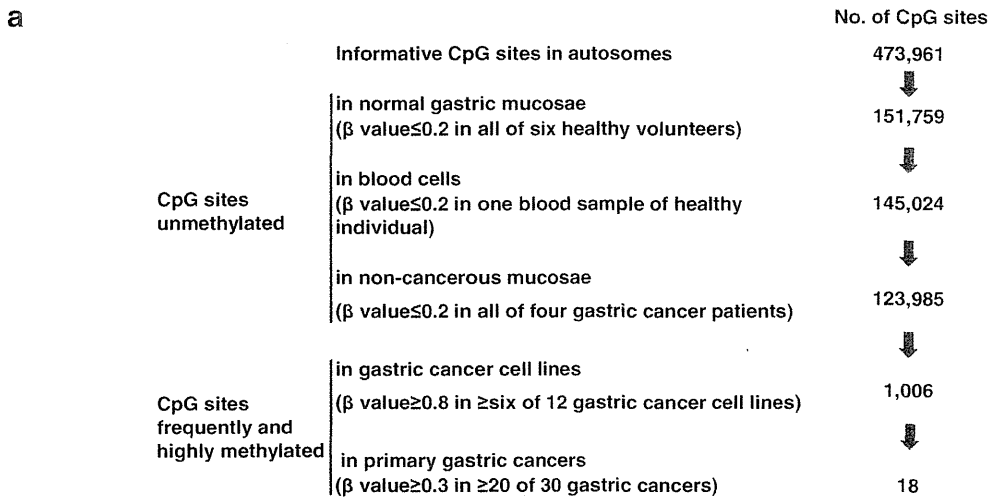

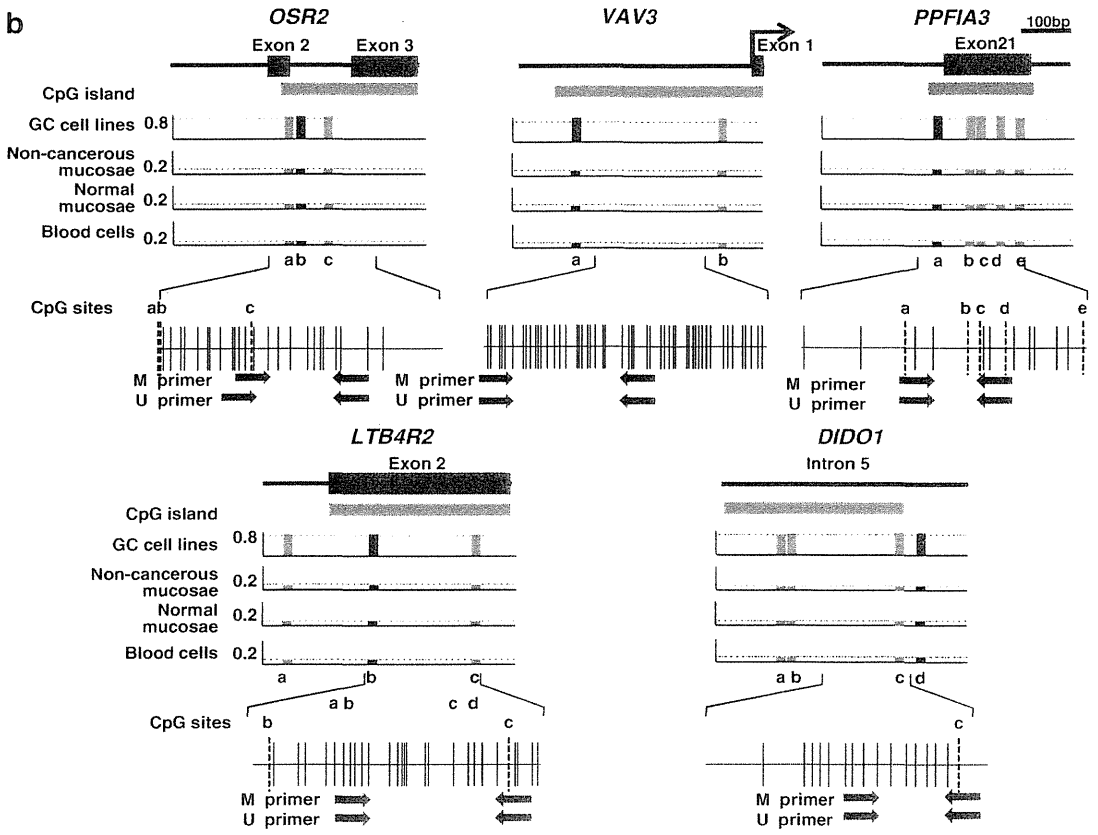

Fig. 1 Selection of specifically methylated regions by a genome-wide screening. **a** Specific genomic regions not methylated in normal cells and fully methylated in cancer cells were selected by a genome-wide screening using an Infinium HumanMethylation450 BeadChip array. Eighteen CpG sites derived from 16 genomic regions were isolated. **b** Five regions of five genes (*OSR2*, *VAV3*, *PPFIA3*, *LTB4R2*, and *DIDO1*) were selected because of their genomic structure and the availability of quantitative methylation-specific PCR (qMSP) primers. The genomic structure, including the location of a CpG island, transcription start site, introns, and exons, is shown at the *top*. The *β* values of the CpG sites analyzed using the bead array are shown in the *middle*, and the *broken lines* show the threshold used in the screening. A CpG map around the CpG site(s) is shown at the *bottom*. *Vertical lines* (*solid* or *broken*) show CpG sites, with *broken lines* showing CpG sites whose *β* values were measured by the bead array. *Arrows* show locations of primers for qMSP. *M* methylated, *U* unmethylated

exclude genes influenced by *H. pylori* infection, the methylation levels of the four genes were analyzed in 23 gastric mucosa samples of *H. pylori*-positive ($n = 14$) and *H. pylori*-negative ($n = 9$) individuals, as well as four samples of peripheral leukocytes different from the one used for the initial screening. The *LTB4R2* methylation level in the *H. pylori*-positive individuals was higher than that in the *H. pylori*-negative individuals and the four samples of peripheral leukocytes, showing that the *LTB4R2* methylation level was affected by *H. pylori* infection. On the other hand, *OSR2*, *VAV3*, and *PPFIA3* were almost unmethylated in the three groups (Fig. 2).

We also analyzed the expression of *OSR2*, *VAV3*, and *PPFIA3* using 17 normal gastric mucosa samples of *H. pylori*-positive ($n = 11$) and *H. pylori*-negative ($n = 6$) individuals. *VAV3* was highly expressed in both *H. pylori*-positive and *H. pylori*-negative gastric mucosae, whereas *OSR2* and *PPFIA3* were only weakly expressed (Fig. S2).

High incidence of methylation of the three genes and their specificity using LCM-purified cells

To examine the incidence of methylation of the three genes in primary GCs, we performed qMSP using 26 independent primary GCs, and observed that at least one of the three genes was methylated in all of the 26 GCs (Fig. 3a). These data showed that if these three genes were used as a panel, they would have a higher coverage (100 %) of primary GCs.

To confirm that the three genes were highly methylated only in GC cells but not in coexisting noncancer cells, four pairs of cancer and noncancer cells were collected by LCM. We found that at least one of the three genes was highly methylated in GC cells (more than 85 %), but that all of them were barely methylated in noncancer cells (less than 5 %) (Fig. 3b). The highest methylation level of the three genes was considered to reflect the fraction of cancer cells, and we defined the panel of the three genes as a DNA methylation marker to estimate the cancer cell fraction in a GC sample.

Because DNA methylation levels of some genes can be influenced by age [24], we also analyzed the correlation between the methylation of the three genes and age. The methylation levels of the three genes were found to be independent of age (Fig. S3).

CNAs of the three genes

CNAs of a marker gene can affect the methylation level of its region in cancer samples [25]. Therefore, we analyzed CNAs of the three regions in the 20 GCs used for the bead array analysis (Fig. 4). *VAV3* and *PPFIA3* showed no CNAs of more than twofold or less than 0.5-fold. In contrast, *OSR2* showed CNAs at low frequencies (more than

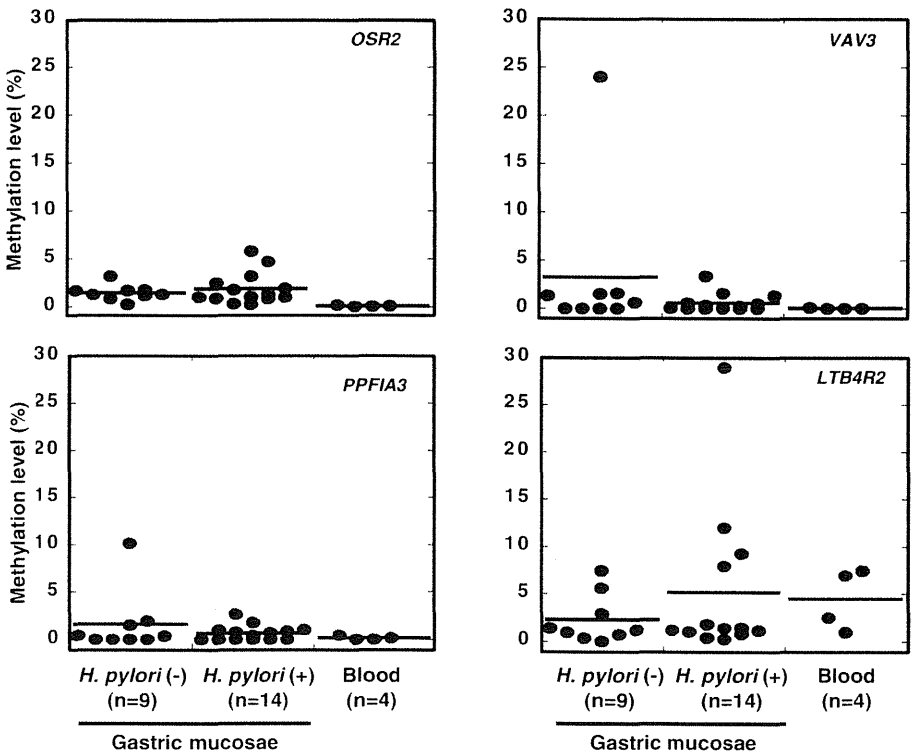

Fig. 2 Isolation of genes not influenced by *Helicobacter pylori* infection. Methylation levels of the four genes were analyzed by quantitative methylation-specific PCR in noncancerous gastric mucosae of *H. pylori*-positive ($n = 14$) and *H. pylori*-negative ($n = 9$) individuals, as well as four samples of peripheral leukocytes. *LTB4R2* was excluded because its methylation level was higher in the *H. pylori*-positive individuals than in the *H. pylori*-negative individuals

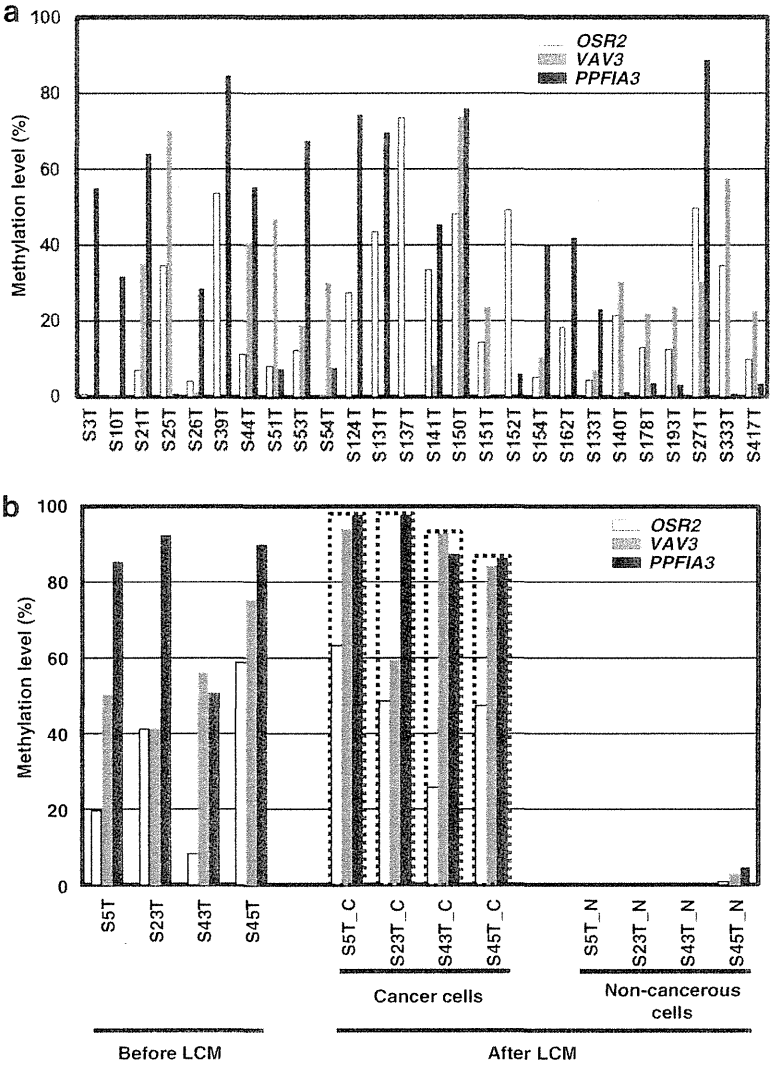

Fig. 3 High incidence of methylation of the three genes and specificity of methylation using cells purified by laser-capture microdissection (LCM). **a** The incidence of hypermethylation of the three genes was analyzed in 26 independent primary gastric cancers (GCs) by quantitative methylation-specific PCR. At least one of the three genes was methylated in all of the 26 GCs. **b** Methylation levels of the three genes were analyzed in four primary GCs before LCM and four pairs of purified cancer and noncancer cells after LCM. At least one of the three genes was highly methylated in GC cells (more than 85 %), but all the three genes were barely methylated in noncancer cells (less than 5 %). *Dotted rectangles* show the panel of the three genes as a DNA methylation marker

twofold in one GC and less than 0.5-fold in two GCs). It was calculated that the deviation of the methylation level from the true cancer cell fraction would be 17.2 % when twofold or 0.5-fold CNA was present in cancer cells [11]. Therefore, the effect of the CNA of *OSR2* was considered to be minimal in the estimation of the cancer cell fraction.

Correlation between the cancer cell fraction estimated by DNA methylation and that estimated by a genetic alteration

To evaluate the accuracy of the DNA methylation marker, 13 GCs with *TP53* mutation were identified among the 30 GCs used for the bead array analysis, and the cancer cell fraction estimated by the marker was compared with the *TP53* mutant frequency. A high correlation between the two methods was observed ($r = 0.77$, $P < 0.001$; Fig. 5). This result showed that the cancer cell fraction estimated by the DNA methylation marker accurately reflected the true fraction of cancer cells in a tumor sample.

Application of the DNA methylation marker to correction of the bead array data

We applied the DNA methylation marker to correct the influence of contamination by normal cells in the data from the epigenomic analysis. For the 30 primary GCs used for the bead array analysis, we measured the fraction of cancer cells using the marker, and corrected the bead array data by division with the evaluated fraction. Unsupervised hierarchical clustering analysis was conducted using 263 genomic blocks selected because their downstream genes

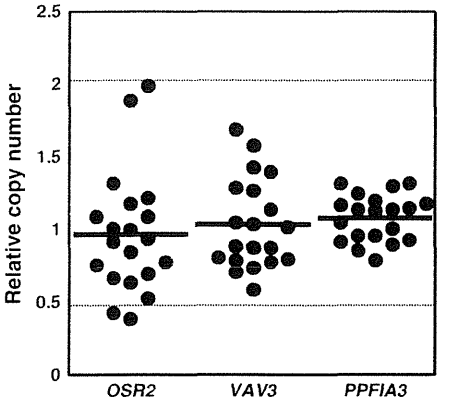

Fig. 4 Copy number alterations (CNAs) of the three genes. CNA of the three genes was analyzed by real-time PCR of the 20 gastric cancers (GCs) used for the bead array analysis. Significant CNA (gain or loss) was defined as a twofold or greater increase or a 0.5-fold or smaller decrease, respectively. Only *OSR2* showed CNAs at low frequencies (twofold or greater in one GC; 0.50-fold or smaller in two GCs)

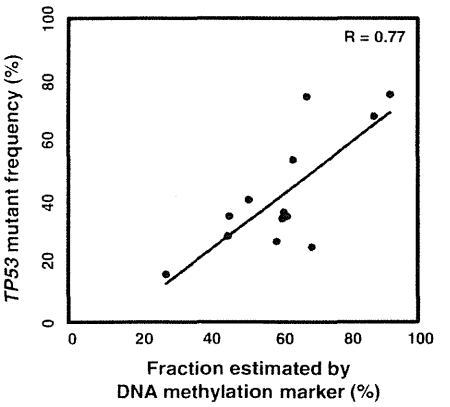

Fig. 5 Correlation between the cancer cell fraction estimated by DNA methylation and that estimated by a genetic alteration. The cancer cell fraction estimated by the DNA methylation marker was compared with the *TP53* mutant frequency. A high correlation between the two methods was observed ($r = 0.77$, $P < 0.001$)

were silenced by aberrant methylation [1] (Fig. 6b). Compared with the heatmap before the correction (Fig. 6a), two samples, S20T and S22T, moved from the CpG island methylator phenotype (CIMP)-negative group to the CIMP-high group. The cancer cell fraction in these two samples was less than 20 % (Fig. 3a). After exclusion of these two samples and correction of the methylation levels, the clustering of the CIMP-high, CIMP-moderate, CIMP-low, and CIMP-negative GCs became much clearer (Fig. 6c). From these data, we concluded that the DNA methylation marker could be used to identify and exclude samples with an extremely low fraction of cancer cells, and to correct the molecular data.

Discussion

We successfully established a panel of three genes (*OSR2*, *VAV3*, and *PPFIA3*) as a marker to estimate the fraction of cancer cells in primary GCs. Using the DNA methylation marker, we were also able to identify and exclude samples with a low fraction of cancer cells, and to correct the methylation levels by the fraction of cancer cells. After this, the genome-wide DNA methylation profiles yielded clearer clustering of CIMP by unsupervised hierarchical clustering analysis. This is the first molecular marker for the cancer cell fraction in GC.

The DNA methylation marker has the advantages of simplicity without the need for experienced pathologists or paired normal samples, compared with microscopic examination and genomic alterations. Also, the DNA methylation marker is likely to have a broad coverage in primary GCs because the DNA methylation marker was methylated in 100 % of the 26 primary GCs used for validation. Further, we were easily able to use the DNA methylation marker to assess the cancer cell fraction, even in diffuse-type GCs, for which even an expert pathologist has difficulty in estimating the cancer cell fraction. Finally, since the methylation levels of the three genes were independent of age, this marker was regarded to be useful to estimate the cancer cell fraction irrespective of age.

The correlation of the cancer cell fraction estimated by the DNA methylation marker with *TP53* mutant frequency was high ($r = 0.77$, $P < 0.001$). However, in two samples, the cancer cell fraction estimated by the marker was twice as large as that estimated by the *TP53* mutant frequency. Since loss of heterozygosity can coexist with a mutation of *TP53* in GCs, we speculated that the discrepancy between the two methods in the two GC samples might have been caused by the loss of heterozygosity of *TP53*.

Gastric mucosae, especially when infected with *H. pylori*, can have very high levels of DNA methylation, so we paid special attention to isolation of marker genes in this study. The panel of the three genes was not affected by *H. pylori* infection because the genes were barely methylated in *H. pylori*-positive mucosae. Only two samples in *H. pylori*-negative individuals had a high methylation of *VAV3* or *PPFIA3*, respectively. One possible reason for detection of such high methylation levels in *H. pylori*-negative samples is that these two samples were contaminated with cancer cells because they were resected from samples from GC patients. Another possible reason is that they were methylated in noncancer cells during past *H. pylori* infection.

A CNA can affect the methylation level of a marker gene. Therefore, we analyzed the CNAs of the three genes in 20 primary GCs used for the bead array analysis, and found CNAs of the three genes had little influence on the

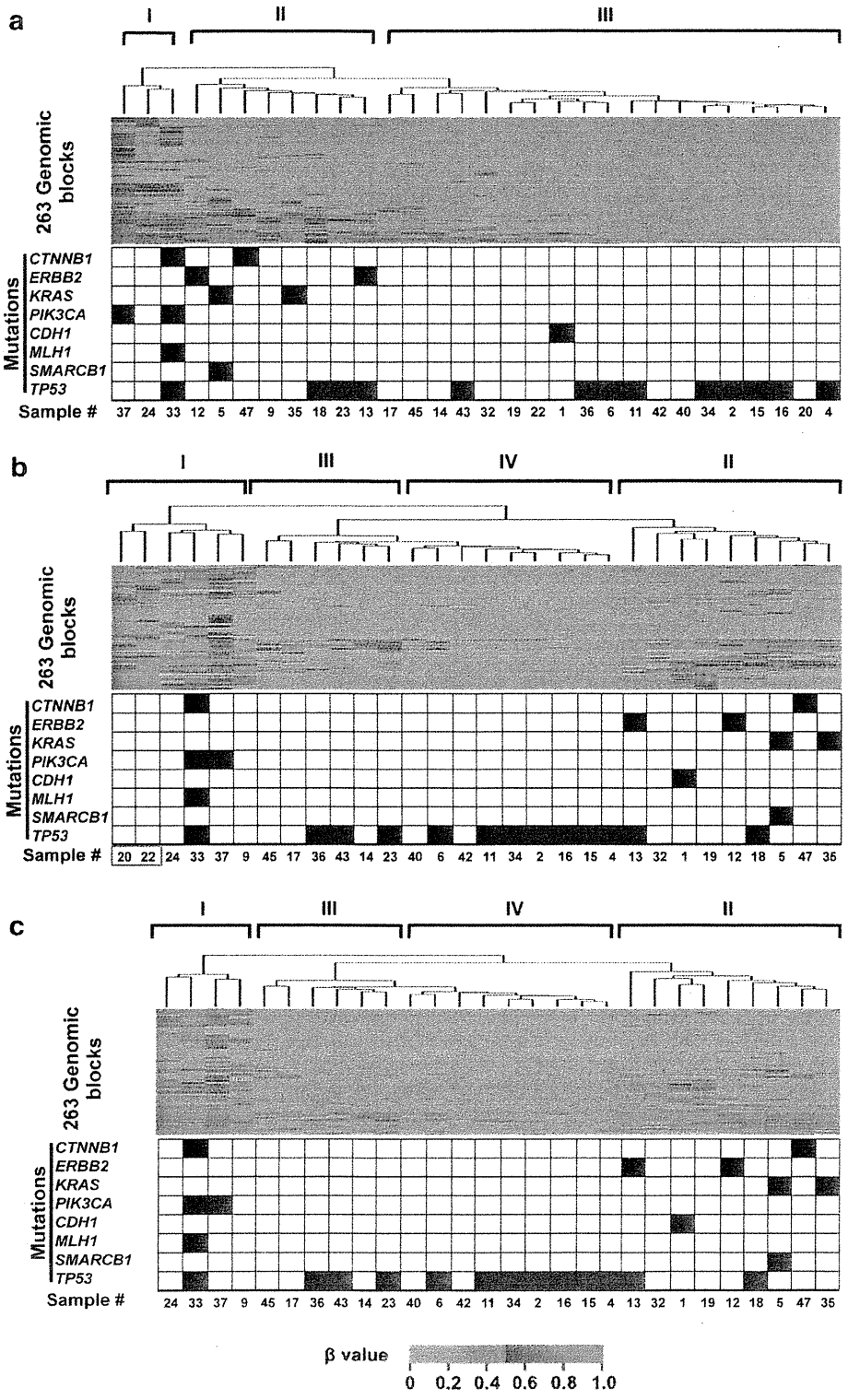

Fig. 6 Application of the DNA methylation marker to the correction of the bead array data. **a** Unsupervised hierarchical clustering analysis of the 30 primary gastric cancers using DNA methylation profiles of 263 genomic blocks. **b** Two samples surrounded by a *red square* (S20T and S22T) moved from the CpG island methylator phenotype (CIMP)-negative group to the CIMP-high group after the Infinium HumanMethylation450 BeadChip array data had been corrected by the DNA methylation marker. **c** After exclusion of two samples with a low fraction of cancer cells, a heatmap using the corrected bead array data showed a much clearer clustering of CIMP-high, CIMP-moderate, CIMP-low, and CIMP-negative gastric cancers

estimation of the cancer cell fraction. Regarding the expression of the three marker genes, only *VAV3* was highly expressed in normal gastric mucosae. The region of *VAV3*, for which DNA methylation was analyzed, was outside the nucleosome-free region, suggesting that its transcription is not necessarily suppressed by the methylation.

In summary, a DNA methylation marker—namely, the panel of the three genes—was isolated, and was shown to be qualified to estimate the cancer cell fraction in GCs. Application of the marker to correction of the bead array data showed promising results for improving the accuracy of molecular analysis. The DNA methylation marker is expected to be useful in many aspects of GC research.

Acknowledgment This work was supported by the Applied Research for Innovative Treatment of Cancer (H26-019) from the Ministry of Health, Labour and Welfare.

Conflict of interest The authors declare that they have no conflict of interest.

References

1. Kim JG, Takeshima H, Niwa T, Rehnberg E, Shigematsu Y, Yoda Y, et al. Comprehensive DNA methylation and extensive mutation analyses reveal an association between the CpG island methylator phenotype and oncogenic mutations in gastric cancers. Cancer Lett. 2013;330:33–40.
2. Letouze E, Martinelli C, Loriot C, Burnichon N, Abermil N, Ottolenghi C, et al. SDH mutations establish a hypermethylator phenotype in paraganglioma. Cancer Cell. 2013;23:739–52.
3. Mudbhary R, Hoshida Y, Chernyavskaya Y, Jacob V, Villanueva A, Fiel MI, et al. UHRF1 overexpression drives DNA hypomethylation and hepatocellular carcinoma. Cancer Cell. 2014;25:196–209.
4. Oue N, Mitani Y, Motoshita J, Matsumura S, Yoshida K, Kuniyasu H, et al. Accumulation of DNA methylation is associated with tumor stage in gastric cancer. Cancer. 2006;106:1250–9.
5. Roma C, Esposito C, Rachiglio AM, Pasquale R, Iannaccone A, Chicchinelli N, et al. Detection of EGFR mutations by TaqMan mutation detection assays powered by competitive allele-specific TaqMan PCR technology. Biomed Res Int. 2013;2013:385087.
6. Meyerson M, Gabriel S, Getz G. Advances in understanding cancer genomes through second-generation sequencing. Nat Rev Genet. 2010;11:685–96.
7. Joseph A, Gnanapragasam VJ. Laser-capture microdissection and transcriptional profiling in archival FFPE tissue in prostate cancer. Methods Mol Biol. 2011;755:291–300.
8. Lin J, Marquardt G, Mullapudi N, Wang T, Han W, Shi M, et al. Lung cancer transcriptomes refined with laser capture microdissection. Am J Pathol. 2014;184(11):2868–84.
9. Carter SL, Cibulskis K, Helman E, McKenna A, Shen H, Zack T, et al. Absolute quantification of somatic DNA alterations in human cancer. Nat Biotechnol. 2012;30:413–21.
10. McFadden DG, Papagiannakopoulos T, Taylor-Weiner A, Stewart C, Carter SL, Cibulskis K, et al. Genetic and clonal dissection of murine small cell lung carcinoma progression by genome sequencing. Cell. 2014;156:1298–311.
11. Takahashi T, Matsuda Y, Yamashita S, Hattori N, Kushima R, Lee YC, et al. Estimation of the fraction of cancer cells in a tumor DNA sample using DNA methylation. PLoS One. 2013;8:e82302.
12. Maekita T, Nakazawa K, Mihara M, Nakajima T, Yanaoka K, Iguchi M, et al. High levels of aberrant DNA methylation in Helicobacter pylori-infected gastric mucosae and its possible association with gastric cancer risk. Clin Cancer Res. 2006;12:989–95.
13. Ushijima T, Hattori N. Molecular pathways: involvement of Helicobacter pylori-triggered inflammation in the formation of an epigenetic field defect, and its usefulness as cancer risk and exposure markers. Clin Cancer Res. 2012;18:923–9.
14. Kang GH, Lee S, Cho NY, Gandamihardja T, Long TI, Weisenberger DJ, et al. DNA methylation profiles of gastric carcinoma characterized by quantitative DNA methylation analysis. Lab Invest. 2008;88:161–70.
15. Lu ZM, Zhou J, Wang X, Guan Z, Bai H, Liu ZJ, et al. Nucleosomes correlate with in vivo progression pattern of de novo methylation of p16 CpG islands in human gastric carcinogenesis. PLoS One. 2012;7:e35928.
16. Yoda Y, Takeshima H, Niwa T, Kim JG, Ando T, Kushima R, et al. Integrated analysis of cancer-related pathways affected by genetic and epigenetic alterations in gastric cancer. Gastric Cancer 2015;18:65–76.
17. Okochi-Takada E, Hattori N, Tsukamoto T, Miyamoto K, Ando T, Ito S, et al. ANGPTL4 is a secreted tumor suppressor that inhibits angiogenesis. Oncogene. 2014;33:2273–8.
18. Tretiakova M, Hart J. Laser microdissection for gene expression study of hepatocellular carcinomas arising in cirrhotic and non-cirrhotic livers. Methods Mol Biol. 2011;755:233–44.
19. Yamashita S, Takahashi S, McDonell N, Watanabe N, Niwa T, Hosoya K, et al. Methylation silencing of transforming growth factor-β receptor type II in rat prostate cancers. Cancer Res. 2008;68:2112–21.
20. Wanajo A, Sasaki A, Nagasaki H, Shimada S, Otsubo T, Owaki S, et al. Methylation of the calcium channel-related gene, CACNA2D3, is frequent and a poor prognostic factor in gastric cancer. Gastroenterology. 2008;135:580–90.
21. Asada K, Ando T, Niwa T, Nanjo S, Watanabe N, Okochi-Takada E, et al. FHL1 on chromosome X is a single-hit gastrointestinal tumor-suppressor gene and contributes to the formation of an epigenetic field defect. Oncogene. 2013;32:2140–9.
22. Kolacsek O, Krizsik V, Schamberger A, Erdei Z, Apati A, Varady G, et al. Reliable transgene-independent method for determining Sleeping Beauty transposon copy numbers. Mob DNA. 2011;2:5.
23. Man TK, Lu XY, Jaeweon K, Perlaky L, Harris CP, Shah S, et al. Genome-wide array comparative genomic hybridization analysis reveals distinct amplifications in osteosarcoma. BMC Cancer. 2004;4:45.
24. Maegawa S, Hinkal G, Kim HS, Shen L, Zhang L, Zhang J, et al. Widespread and tissue specific age-related DNA methylation changes in mice. Genome Res. 2010;20:332–40.
25. Robinson MD, Stirzaker C, Statham AL, Coolen MW, Song JZ, Nair SS, et al. Evaluation of affinity-based genome-wide DNA methylation data: effects of CpG density, amplification bias, and copy number variation. Genome Res. 2010;20:1719–29.

Katsurada et al. SpringerPlus 2014, 3:620
http://www.springerplus.com/content/3/1/620

SpringerPlus
a SpringerOpen Journal

RESEARCH Open Access

High-sensitivity troponin T as a marker to predict cardiotoxicity in breast cancer patients with adjuvant trastuzumab therapy

Kenichi Katsurada[1], Masaru Ichida[1*], Masako Sakuragi[2], Megumi Takehara[2], Yasuo Hozumi[2] and Kazuomi Kario[1]

Abstract

The humanized monoclonal antibody trastuzumab has been in routine use for chemotherapy for human epidermal growth factor receptor II (HER2)-positive breast cancer. A major adverse effect of trastuzumab is cardiotoxicity. Well-established biomarkers or echocardiographic parameters to predict trastuzumab-induced cardiotoxicity have not yet been determined. We attempted to identify useful biomarkers and/or echocardiographic parameters to predict trastuzumab-induced cardiotoxicity.

We prospectively investigated the cases of 19 women who received chemotherapy including anthracyclines and trastuzumab for HER2-positive breast cancer. We measured cardiac biomarkers and echocardiographic parameters before their chemotherapy and every 3 months up to 15 months until the end of the adjuvant trastuzumab therapy.

We divided the patients into two groups: group R was the nine patients who showed a reduction of left ventricular ejection fraction (LVEF) ≥5%, and group N was the 10 patients who showed a reduction of LVEF <5%. The high-sensitivity troponin T (hs-TnT) level at 6 months was significantly higher in group R than in group N (11.0 ± 7.8 pg/mL vs. 4.0 ± 1.4 pg/mL, $p < 0.01$). The hs-TnT level with a cutoff value of 5.5 pg/mL at 6 months had 78% sensitivity and 80% specificity for predicting a reduction of LVEF at 15 months. In our evaluation of echocardiographic parameters at baseline, the diastolic function was more impaired in group R than in group N.

The hs-TnT and echocardiographic parameters of diastolic function could be useful to predict trastuzumab-induced cardiotoxicity.

Keywords: Trastuzumab; Anthracycline; Chemotherapy; Cardiotoxicity; Heart failure; Cardiac Troponin; Biomarker; Echocardiography

Background

Trastuzumab is a humanized monoclonal antibody that has been in routine use for chemotherapy for human epidermal growth factor receptor II (HER2)-positive breast cancer. Several clinical trials revealed evidence that combination therapy with trastuzumab and anthracyclines improved the survival rate of patients with HER2-positive breast cancer, which is detected in 20% to 30% of all breast cancers and has both a poor prognosis and a high risk of recurrence (Hudis 2007). However, a known major adverse effect of trastuzumab is cardiotoxicity, which can cause the development of heart failure and necessitate the withdrawal of a therapeutic agent for breast cancer (Chen et al. 2008). The assessment of a reduction of the ventricular ejection fraction (LVEF) by echocardiography or cardiac scintigraphy has been used to detect trastuzumab induced-cardiotoxicity. It is an important issue to elucidate the markers to predict trastuzumab-induced cardiotoxicity before which show a reduction of LVEF.

Several reports showed that plasma concentration of high-sensitivity troponin I (hs-TnI) or a myocardial strain measured by echocardiography correlates with the risk of trastuzumab-induced cardiotoxicity, and thus the measurement of these parameters may be able to predict cardiotoxicity (Sawaya et al. 2011, 2012; Fallah-Rad et al. 2011). However, specific biomarkers or echocardiographic

* Correspondence: bcichida@jichi.ac.jp
[1]Department of Cardiology, Jichi Medical University School of Medicine, 3311-1 Yakushiji, Shimotsuke, Tochigi 329-0498, Japan
Full list of author information is available at the end of the article

parameters to predict trastuzumab-induced cardiotoxicity remains to be established.

In this study, we prospectively investigated whether cardiac biomarkers and/or echocardiographic parameters predict the incidence of trastuzumab-induced cardiotoxicity, and we compared the operating characteristics of these parameters with those reported before.

Methods

Study design and patient selection

Twenty women with HER2-positive breast cancer and scheduled to receive adjuvant chemotherapy including anthracyclines, taxanes and trastuzumab at Jichi Medical University Hospital between June 2010 and March 2012 were prospectively enrolled. The patient population was evaluated before chemotherapy and every 3 months up to 15 months until the end of trastuzumab therapy: before the initiation of anthracycline therapy (at baseline), the completion of the anthracycline therapy (before the initiation of trastuzumab therapy: at 3 months), and at 6, 9, 12 and 15 months. At each time point, cardiac biomarkers and echocardiographic parameters were measured (Figure 1).

In accordance with the guideline of the Cardiac Review and Evaluation Committee for trastuzumab-associated cardiotoxicity, we defined trastuzumab-induced cardiotoxicity as a reduction of LVEF ≥5% to <55% with symptomatic heart failure or an asymptomatic reduction of LVEF ≥10% to <55%. Because none of the present 20 patients showed cardiotoxicity in accordance with this definition, we defined cardiac damage as a reduction of LVEF ≥5%, and we divided the patients into two groups: group R (reduction of LVEF ≥5%) and group N (reduction of LVEF <5%) for analysis. The Ethics Committee of Jichi Medical University approved the study protocol. All patients enrolled in this study provided informed consent.

Measurement of biomarkers

The biomarkers assessed in this study were high-sensitivity troponin T (hs-TnT), high-sensitivity troponin I (hs-TnI), high-sensitivity C-reactive protein (hs-CRP), N-terminal pro-brain natriuretic peptide (NT-proBNP), serum creatinine (Cr), and the estimated glomerular filtration rate (eGFR). The levels of hs-TnT, hs-CRP and NT-proBNP were measured by an electrochemiluminescence immunoassay, latex-enhanced nephelometry, and an electrochemiluminescence sandwich immunoassay, respectively, according to the manufacturer's instructions (Roche Diagnostics, Mannheim, Germany). The hs-TnT assay has an analytic range of 3–10,000 pg/mL, and the 99th percentile cutoff point has been reported as ≥14 pg/mL in healthy individuals (Giannitsis et al. 2010). The hs-TnI levels were measured using a chemiluminescence sandwich immunoassay according to the manufacturer's instructions (Siemens Medical Solution Diagnostics, Tarrytown NY, USA). The hs-TnI assay has an analytic range of 6–50,000 pg/mL, and the 99th percentile cutoff point has been reported as ≥40 pg/mL in healthy individuals (Melanson et al. 2007). Cr was determined by a standard assay at Jichi Medical University Hospital, and the eGFR was calculated by the method defined by the Japan Association of Chronic Kidney Disease ($eGFR = 194 \times Cr^{-1.094} \times age^{-0.287} \times 0.739$).

Measurement of echocardiographic parameters

Transthoracic echocardiography was performed using the iE33 (Philips, Eindhoven, Netherlands) or ARTIDA (Toshiba Medical Systems Corp., Tochigi, Japan). All echocardiographic examinations were performed by experienced cardiologists (K.K. and M.I.) blinded to the biomarker results. Echocardiographic parameters were measured in accordance with the guidelines of the American Society of Echocardiography, and the following parameters were assessed: LVEF, left ventricular end-diastolic diameter (LVDd), mitral E-wave filling velocity/mitral A-wave filling velocity (E/A), deceleration time (DcT), peak early diastolic velocity of septal mitral annulus (e').

LVEF was measured by a modified Simpson's method except in one patient. Because this patient's apical view was difficult to visualize due to expanders, the LVEF was measured by the M-mode method using the

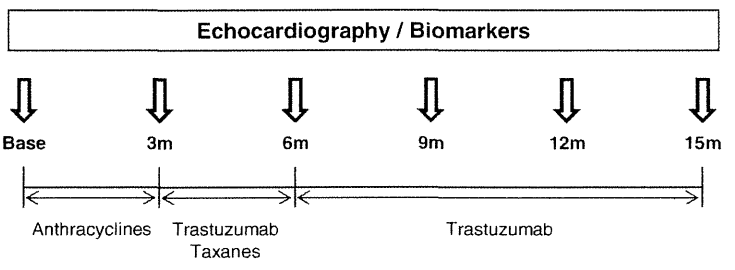

Figure 1 Time course of the study protocol. Base: baseline; m: months

parasternal view, and the E/A, DcT, and e' could not be evaluated.

Statistical analysis

All data are expressed as the mean ± SD. Categorical variables are expressed as percentages and were analyzed using the χ-square test or Fisher's exact test. The variables that were not normally distributed were logarithmically transformed before the analysis. The comparisons of variables between group N and group R at the same time points were done with Student's *t*-tests. The comparison of variables within each group versus the baseline was performed with a repeated-measures analysis of variance (ANOVA) followed by Tukey's test. Pearson's correlation was used to test relationship between the changes of hs-TnT and LVEF. A receiver-operator characteristic (ROC) curve analysis was applied to determine the cutoff values, sensitivity and specificity for hs-TnT. A *p*-value <0.05 was considered significant. The software program SPSS (version 16.0, Chicago, IL) was used to perform the analysis.

Results

Twenty women were prospectively enrolled in this study; one patient was excluded from the study because her chemotherapy protocol was changed because a malignant lymphoma developed during her breast cancer treatment. Therefore, 19 patients participated in and completed the study. They were divided into two groups: group R was nine patients and group N was 10 patients.

The baseline characteristics are listed in Table 1. The body mass index values were significantly higher in group R than in group N (25 ± 3 vs. 22 ± 2, $p < 0.05$). There was no significant difference between the two groups in age, cardiovascular risk factors, side of breast cancer, radiation use, dose of anthracyclines, or renal function. In the evaluation of echocardiographic parameters at baseline, there was no significant difference in LVEF or LVDd between the two groups. The E/A and e' values were significantly lower in group R than in group N (1.00 ± 0.36 vs. 1.44 ± 0.41, $p < 0.05$ and 7.6 ± 2.0 cm/s vs. 11.2 ± 3.2 cm/s, $p < 0.05$, respectively), and DcT was

Table 1 Baseline characteristics of the 19 patients with HER2-positive breast cancer who showed normal (N) or reduced (R) left ventricular ejection fraction

	Group N (n = 10)	Group R (n = 9)	*p-value*
Age (yrs)	49 ± 7	57 ± 9	0.071
Body mass index (kg/m2)	22 ± 2	25 ± 3	0.037
Cardiovascular risk factors			
Hypertension	1 (10%)	1 (11%)	0.941
Diabetes	0 (0%)	0 (0%)	
Hyperlipidemia	2 (20%)	2 (22%)	0.912
Smoking	2 (20%)	4 (44%)	0.277
Family history of CAD	1 (10%)	0 (0%)	0.357
Side of breast cancer			
Right	6 (60%)	8 (89%)	0.171
Left	4 (40%)	1 (11%)	
Bilateral	0 (0%)	0 (0%)	
Radiation	7 (70%)	5 (56%)	0.541
Chemotherapy			
Doxorubicin 240 mg/m2	1 (10%)	4 (44%)	0.098
Epirubicin 300 mg/m2	9 (90%)	5 (56%)	
Creatinine (mg/dL)	0.55 ± 0.10	0.50 ± 0.07	0.225
eGFR (mL/min/1.73 m2)	93.9 ± 19.0	100.5 ± 21.1	0.509
Echocardiographic parameters			
LVEF (%)	68 ± 5	71 ± 3	0.103
LVDd (mm)	44 ± 3	44 ± 4	0.756
E/A	1.44 ± 0.41	1.00 ± 0.36	0.028
DcT (ms)	185 ± 26	227 ± 48	0.040
e' (cm/s)	11.2 ± 3.2	7.6 ± 2.0	0.019

CAD: coronary artery disease, eGFR: estimated glormerular filtration rate, LVEF: left ventricular ejection fraction, LVDd: left ventricular end-diastolic diameter, E/A: mitral E-wave filling velocity/mitral A-wave filling velocity, DcT: deceleration time, e': peak early diastolic velocity of septal mitral annulus.

significantly longer in group R than in group N (227 ± 48 ms vs. 185 ± 26 ms, $p < 0.05$), showing that diastolic function was more impaired in group R than in group N.

The changes of LVEF at 3, 6, 9, 12 and 15 months versus baseline are shown in Figure 2. At 9, 12 and 15 months, the LVEF was significantly reduced in group R compared to group N. In group R, the LVEF was significantly reduced at 6, 9, 12, and 15 months compared to baseline, whereas in group N, the LVEF was not changed at any time point. The reduction of LVEF at 15 months in group R was 9%.

The changes in cardiac biomarkers are shown in Table 2. In group R, the hs-TnT levels were significantly elevated at 3 and 6 months compared to baseline. In group N, the hs-TnT levels were significantly elevated at 3 months compared to baseline. At 6 months, the hs-TnT levels in group R were significantly higher than those in group N (11.0 ± 7.8 pg/mL vs. 4.0 ± 1.4 pg/mL, $p < 0.01$).

In group R, the hs-TnI levels were significantly elevated at 3, 6, 12 and 15 months compared to baseline. In group N, the hs-TnI levels were significantly elevated at 3, 6 and 15 months compared to baseline. There was no significant difference in hs-TnI levels between the two groups at any time point.

In both group R and group N, the hs-CRP levels were significantly elevated at 3 months compared to baseline. There was no significant difference in hs-CRP levels between the two groups at any time point.

In both group R and group N, the NT-proBNP levels were not significantly different from the baseline levels at any time point. There was no significant difference in NT-proBNP levels between the two groups at any time point.

Figure 3A shows the changes of hs-TnT levels at 6 months significantly correlated with the changes of LVEF at 15 months (r = −0.56, $p < 0.05$). The distribution of hs-TnT levels at 6 months and the ROC curve analysis of hs-TnT levels at 6 months are shown in Figure 3B and Figure 3C, respectively. At 6 months, seven of the nine patients in group R were above the hs-TnT cutoff value of 5.5 pg/mL, providing 78% sensitivity and 80% specificity for predicting a reduction of LVEF at 15 months.

Discussion

In this study's search for predictors of cardiotoxicity in breast cancer treatment, two findings are notable. First, elevated hs-TnT levels at 6 months showed a possible ability to predict a subsequent reduction of LVEF. Second, the cardiac diastolic function at baseline was more impaired in group R than in group N.

Cardiac troponins are contractile regulatory peptides, and with cardiac muscle injury they spill into circulating blood. They are used as diagnostic biomarkers, especially for acute coronary syndrome (Donnelly and Millar-Craig 1998; Antman et al. 1996; Apple et al. 2005; Aviles et al. 2002; Lindahl et al. 2000). A high-sensitivity cardiac troponin assay that can detect low levels of circulating cardiac troponin has emerged, and its diagnostic and prognostic accuracy have been reported in several groups of patients with cardiovascular diseases such as subclinical cardiovascular diseases (deFilippi et al. 2010), heart failure (Latini et al. 2007), and stable coronary artery disease (Omland et al. 2009). This high-sensitivity troponin assay can measure two kinds of troponin, troponin T and I. There are several differences between troponin T and I; for example, troponin T has a larger

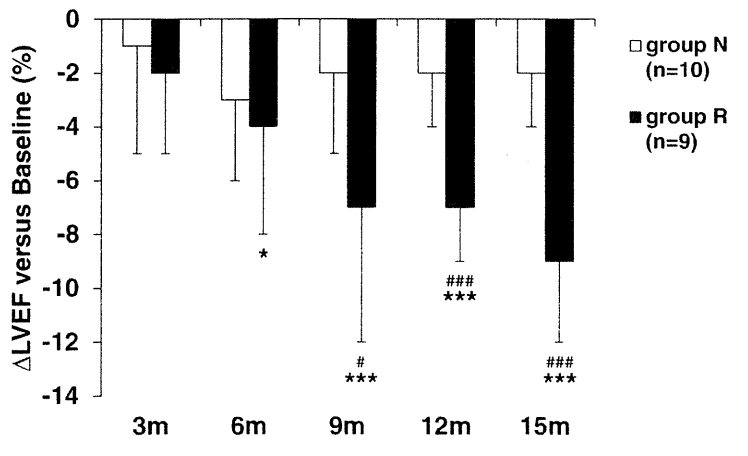

Figure 2 The changes of left ventricular ejection fraction (ΔLVEF) at 3 months (3 m), 6 months (6 m), 9 months (9 m), 12 months (12 m) and 15 months (15 m) versus baseline. Bars represent mean ± SD. $^{\#}p < 0.05$, $^{\#\#}p < 0.01$ and $^{\#\#\#}p < 0.001$ comparing group N vs. group R at the same time point. $^{*}p < 0.05$, $^{**}p < 0.01$ and $^{***}p < 0.001$ within each group vs. baseline with a repeated ANOVA followed by Tukey's test.

Table 2 Biomarker levels in the HER2-positive breast cancer patients who showed normal (N) or reduced (R) left ventricular ejection fraction

Biomarkers	Group N (n = 10)	Group R (n = 9)	*p-value*
hs-TnT (pg/mL)			
Baseline	3.0	3.0	
3 months	7.0 ± 5.8**	9.2 ± 6.6*	0.524
6 months	4.0 ± 1.4	11.0 ± 7.8**	0.005
9 months	4.4 ± 2.7	3.6 ± 1.7	0.457
12 months	3.9 ± 1.6	4.9 ± 2.1	0.321
15 months	3.8 ± 1.0	4.4 ± 2.1	0.588
hs-TnI (pg/mL)			
Baseline	4.2 ± 4.0	2.8 ± 2.9	0.426
3 months	14.1 ± 7.0***	19.7 ± 17.3***	0.649
6 months	10.6 ± 6.7**	21.6 ± 16.4***	0.246
9 months	7.3 ± 4.8	7.3 ± 6.1	0.621
12 months	7.8 ± 5.9	8.7 ± 5.0 **	0.634
15 months	10.3 ± 3.5**	10.9 ± 6.4***	0.788
hs-CRP (mg/dL)			
Baseline	0.04 ± 0.02	0.14 ± 0.18	0.112
3 months	0.35 ± 0.27*	0.71 ± 0.64*	0.283
6 months	0.09 ± 0.09	0.11 ± 0.12	0.393
9 months	0.04 ± 0.03	0.05 ± 0.03	0.521
12 months	0.18 ± 0.42	0.08 ± 0.11	0.867
15 months	0.07 ± 0.07	0.85 ± 1.43	0.219
NT-proBNP (pg/mL)			
Baseline	66.0 ± 30.5	46.6 ± 43.5	0.071
3 months	56.4 ± 41.9	99.4 ± 76.9	0.337
6 months	45.3 ± 32.8	22.9 ± 13.5	0.112
9 months	39.5 ± 27.4	59.1 ± 27.2	0.093
12 months	59.9 ± 51.4	52.1 ± 28.0	0.886
15 months	61.1 ± 44.0	52.9 ± 26.4	0.795

*p < 0.05, **p < 0.01 and ***p < 0.001 vs. baseline within each group with a repeated ANOVA followed by Tukey's test.

molecular weight and a longer half-life in blood, and it is more affected by renal dysfunction than troponin I (Tsutamoto et al. 2009, 2010; Fehr et al. 2003). A recent report discussed the differences between the roles of troponin T and I in the prediction of cardiovascular events in stable coronary artery disease patients, and in that report, hs-TnI correlated moderately with hs-TnT (r = 0.44), and hs-TnI was associated with the incidence of myocardial infarction (Omland et al. 2013).

Our study is the first to reveal that in group R, both the hs-TnT levels and the hs-TnI levels not only at 3 months but also at 6 months were significantly higher than the corresponding values at baseline. Sawaya et al. (2012) reported the utility of hs-TnI to predict trastuzumab-induced cardiotoxicity. Their report showed that elevated hs-TnI levels at 3 months after the completion of anthracycline therapy could predict subsequent cardiotoxicity in breast cancer patients with adjuvant trastuzumab therapy, and that hs-TnI with a cutoff value of 30 pg/mL had 48% sensitivity and 73% specificity for detecting cardiotoxicity. However, when we look into the report in detail, Sawaya's report showed that there were no significant differences in hs-TnI levels between the group with cardiotoxicity and the group without cardiotoxicity (32 pg/mL vs. 17 pg/mL, $p = 0.18$). In our study, the hs-TnT levels but not the hs-TnI levels at 6 months were significantly different between the two groups (11.0 ± 7.8 pg/mL vs. 4.0 ± 1.4 pg/mL, $p < 0.01$), and hs-TnT with a cutoff value of 5.5 pg/mL was predictive of a subsequent reduction of LVEF by nearly 10% at 15 months, suggesting that hs-TnT could be a more useful marker to predict cardiotoxicity than hs-TnI. The molecular size of troponin I is smaller than that of troponin T, which may facilitate transfer of troponin I spill into circulating blood, and induce a large variation in the hs-TnI levels of group N. This may indicate that the leakage of troponin T could more specifically reflect severe myocardial damage causing reduction of LVEF.

It is a novel finding that a continuous elevation of high-sensitivity troponins at 3 and 6 months, not only at 3 months, is correlated with the subsequent development of cardiotoxicity. Anthracycline therapy for breast cancer patients is generally completed at 3 months and then adjuvant trastuzumab therapy is initiated, and our results thus suggest that anthracycline-induced cardiotoxicity remains and trastuzumab-induced myocardial injury is added at 6 months. Trastuzumab is thought to inhibit a process of repairing myocardial injury caused by anthracyclines, leading to a subsequent reduction of LVEF. This hypothesis is in agreement with the previous report that the incidence of cardiotoxicity ranges from 2% to 7% when trastuzumab is used as a monotherapy, and up to 27% when trastuzumab is used with anthracyclines as adjuvant therapy (Yeh and Bickford 2009).

Onitilo et al. (2012) showed that elevated hs-CRP (≥0.3 mg/dL) during trastuzumab therapy had 93% sensitivity and 46% specificity for detecting cardiotoxicity, and that this value was useful especially for identifying patients at low risk of developing cardiotoxicity. Our study also showed that hs-CRP levels were significantly elevated at 3 months compared to baseline, although there were no significant differences between the two patient groups. This result is in agreement with Onitilo's report and might reflect inflammations due to anthracycline-induced cardiotoxicity. On the other hand, in our study as well as in several previous reports (Sawaya et al. 2011, 2012; Fallah-Rad et al. 2011), the NT-proBNP levels of both group R and group N patients were not significantly different compared to those at baseline at any time points.

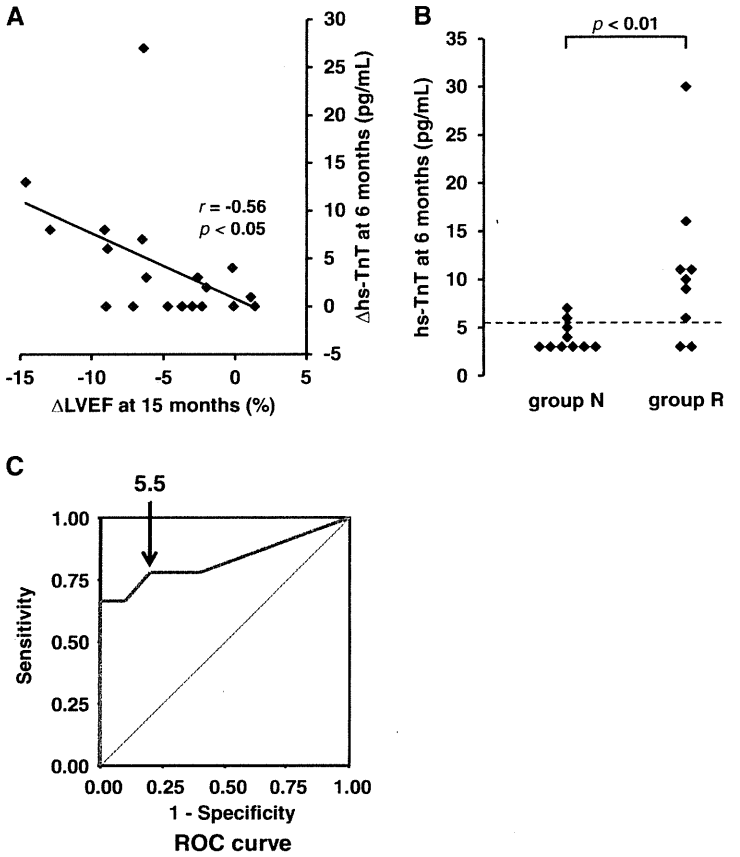

Figure 3 The hs-TnT level at 6 months predicts a reduction of LVEF at 15 months. (A) The correlation between the changes of high-sensitivity troponin T (Δhs-TnT) at 6 months and the changes of left ventricular ejection fraction (ΔLVEF) at 15 months. **(B)** The dot diagram depicting the distribution of hs-TnT at 6 months in each group. **(C)** The ROC curve analysis of hs-TnT at 6 months in both groups. The transverse dot line in **(B)** and the arrow in **(C)** indicate the cutoff point of hs-TnT that provides the maximum value by adding sensitivity to specificity.

Our study is the first to show that the diastolic function at baseline was more impaired in group R than in group N. Several studies indicated the utility of decreased longitudinal strain (Sawaya et al. 2011, 2012; Fallah-Rad et al. 2011) and systolic velocity of septal mitral annulus (s') (Fallah-Rad et al. 2011) measured by echocardiography for predicting the cardiotoxicity of adjuvant trastuzumab therapy. In our study, s' was not significantly different at any time point because there was no patient with severe systolic dysfunction such as reduction of LVEF ≥10% to <55% (data not shown). However, we showed that at baseline, the E/A and e' values were significantly lower and the DcT was significantly longer in group R than in group N, suggesting that echocardiographic parameters of diastolic function could be useful to identify patients at high risk of developing cardiotoxicity. These findings seem to be supported by some previous reports showing that diastolic dysfunction precedes or coexists with systolic dysfunction for various conditions, such as hypertensive heart disease and ischemic heart disease (Vasan and Levy 1996; Nishimura and Tajik 1997).

Our study has several limitations. First, we used a reduction of LVEF ≥5% as a surrogate marker of trastuzumab-induced cardiotoxicity. None of our patients developed heart failure, and the incidence of trastuzumab-induced cardiotoxicity was lower than in some other previous studies. The following points can be given as the reasons. In our patient population, the prevalence of underlying diseases such as diabetes, hypertension and obesity were lower than those in previous studies. These diseases are known to be conventional cardiac risk factors and have been reported as robust predictors of anthracycline-induced cardiotoxicity (Lotrionte et al. 2013). Another point was that the sensitivity for chemotherapy-induced cardiotoxicity could be different between races. In addition, myocardial strains measured by echocardiography were not assessed in our study. Moreover, our study was prospective but the population was small. Further studies

with larger populations are needed to test the significance of hs-TnT in trastuzumab-induced cardiotoxicity.

Conclusions

Our study clearly showed that the continuous elevation of hs-TnT at 3 and 6 months during adjuvant trastuzumab therapy could predict the subsequent reduction of LVEF, and diastolic function at baseline was more impaired in group R than in group N. In breast cancer patients treated with anthracyclines and trastuzumab, hs-TnT and echocardiographic parameters of diastolic function may be useful to predict cardiotoxicity, and they may be helpful as guides to avoid adverse cardiac effects.

Competing interests

The authors declare that they have no competing interest.

Authors' contributions

KK: Protocol development, Data collection, Data management, Data analysis, Manuscript writing and editing. MI: Protocol development, Data collection, Data management, Data analysis, Manuscript editing. MS: Data collection. MT: Data collection. YH: Protocol development, Data collection, Manuscript editing. KK: Manuscript editing. All authors read and approved the final manuscript.

Acknowledgments

We thank Kimiyo Saito for her excellent technical assistance.

Author details

[1]Department of Cardiology, Jichi Medical University School of Medicine, 3311-1 Yakushiji, Shimotsuke, Tochigi 329-0498, Japan. [2]Department of Breast Oncology, Jichi Medical University School of Medicine, 3311-1 Yakushiji, Shimotsuke, Tochigi 329-0498, Japan.

Received: 7 October 2014 Accepted: 8 October 2014
Published: 20 October 2014

References

Antman EM, Tanasijevic MJ, Thompson B, Schactman M, McCabe CH, Cannon CP, Fischer GA, Fung AY, Thompson C, Wybenga D, Braunwald E (1996) Cardiac-specific troponin I levels to predict the risk of mortality in patients with acute coronary syndromes. N Engl J Med 335:1342–1349

Apple FS, Wu AH, Mair J, Ravkilde J, Panteghini M, Tate J, Pagani F, Christenson RH, Mockel M, Danne O, Jaffe AS, Committee on Standardization of Markers of Cardiac Damage of the IFCC (2005) Future biomarkers for detection of ischemia and risk stratification in acute coronary syndrome. Clin Chem 51:810–824

Aviles RJ, Askari AT, Lindahl B, Wallentin L, Jia G, Ohman EM, Mahaffey KW, Newby LK, Califf RM, Simoons ML, Topol EJ, Berger P, Lauer MS (2002) Troponin T levels in patients with acute coronary syndromes, with or without renal dysfunction. N Engl J Med 346:2047–2052

Chen MH, Kerkela R, Force T (2008) Mechanism of cardiac dysfunction associated with tyrosine kinase inhibitor cancer therapeutics. Circulation 118:84–95

deFilippi CR, de Lemos JA, Christenson RH, Gottdiener JS, Kop WJ, Zhan M, Seliger SL (2010) Association of serial measures of cardiac troponin T using a sensitive assay with incident heart failure and cardiovascular mortality in older adults. JAMA 304:2494–2502

Donnelly R, Millar-Craig MW (1998) Cardiac troponins: IT upgrade for the heart. Lancet 351:537–539

Fallah-Rad N, Walker JR, Wassef A, Lytwyn M, Bohonis S, Fang T, Tian G, Kirkpatrick ID, Singal PK, Krahn M, Grenier D, Jassal DS (2011) The utility of cardiac biomarkers, tissue velocity and strain imaging, and cardiac magnetic resonance imaging in predicting early left ventricular dysfunction in patients with human epidermal growth factor receptor II-positive breast cancer treated with adjuvant trastuzumab therapy. J Am Coll Cardiol 57:2263–2270

Fehr T, Knoflach A, Ammann P, Pei P, Binswanger U (2003) Differential use of cardiac troponin T versus I in hemodialysis patients. Clin Nephrol 59:35–39

Giannitsis E, Kurz K, Hallermayer K, Jarausch J, Jaffe AS, Katus HA (2010) Analytical validation of a high-sensitivity cardiac troponin T assay. Clin Chem 56:254–261

Hudis CA (2007) Trastuzumab — mechanism of action and use in clinical practice. N Engl J Med 357:39–51

Latini R, Masson S, Anand IS, Missov E, Carlson M, Vago T, Angelici L, Barlera S, Parrinello G, Maggioni AP, Tognoni G, Cohn JN, Investigators V-HFT (2007) Prognostic value of very low plasma concentrations of troponin T in patients with stable chronic heart failure. Circulation 116:1242–1249

Lindahl B, Toss H, Siegbahn A, Venge P, Wallentin L, Markers of myocardial damage and inflammation in relation to long-term mortality in unstable coronary artery disease. FRISC Study Group (2000) Fragmin during Instability in Coronary Artery Disease. N Engl J Med 343:1139–1147

Lotrionte M, Biondi-Zoccai G, Abbate A, Lanzetta G, D'Ascenzo F, Malavasi V, Peruzzi M, Frati G, Palazzoni G (2013) Review and meta-analysis of incidence and clinical predictors of anthracycline cardiotoxicity. Am J Cardiol 112:1980–1984

Melanson SE, Morrow DA, Jarolim P (2007) Earlier detection of myocardial injury in a preliminary evaluation using a new troponin I assay with improved sensitivity. Am J Clin Pathol 128:282–286

Nishimura RA, Tajik AJ (1997) Evaluation of diastolic filling of left ventricle in health and disease: Doppler echocardiography is the clinician's Rosetta Stone. J Am Coll Cardiol 30:8–18

Omland T, de Lemos JA, Sabatine MS, Christophi CA, Rice MM, Jablonski KA, Tjora S, Domanski MJ, Gersh BJ, Rouleau JL, Pfeffer MA, Braunwald E, Prevention of Events with Angiotensin Converting Enzyme Inhibition (PEACE) Trial Investigators (2009) A sensitive cardiac troponin T assay in stable coronary artery disease. N Engl J Med 361:2538–2547

Omland T, Pfeffer MA, Solomon SD, de Lemos JA, Røsjø H, Šaltytė Benth J, Maggioni A, Domanski MJ, Rouleau JL, Sabatine MS, Braunwald E, Investigators PEACE (2013) Prognostic value of cardiac troponin I measured with a highly sensitive assay in patients with stable coronary artery disease. J Am Coll Cardiol 61:1240–1249

Onitilo AA, Engel JM, Stankowski RV, Liang H, Berg RL, Doi SA (2012) High-sensitivity C-reactive protein (hs-CRP) as a biomarker for trastuzumab-induced cardiotoxicity in HER2-positive early-stage breast cancer: a pilot study. Breast Cancer Res Treat 134:291–298

Sawaya H, Sebag IA, Plana JC, Januzzi JL, Ky B, Cohen V, Gosavi S, Carver JR, Wiegers SE, Martin RP, Picard MH, Gerszten RE, Halpern EF, Passeri J, Kuter I, Scherrer-Crosbie M (2011) Early detection and prediction of cardiotoxicity in chemotherapy-treated patients. Am J Cardiol 107:1375–1380

Sawaya H, Sebag IA, Plana JC, Januzzi JL, Ky B, Tan TC, Cohen V, Banchs J, Carver JR, Wiegers SE, Martin RP, Picard MH, Gerszten RE, Halpern EF, Passeri J, Kuter I, Scherrer-Crosbie M (2012) Assessment of echocardiography and biomarkers for the extended prediction of cardiotoxicity in patients treated with anthracyclines, taxanes, and trastuzumab. Circ Cardiovasc Imaging 5:596–603

Tsutamoto T, Kawahara C, Yamaji M, Nishiyama K, Fujii M, Yamamoto T, Horie M (2009) Relationship between renal function and serum cardiac troponin T in patients with chronic heart failure. Eur J Heart Fail 11:653–658

Tsutamoto T, Kawahara C, Nishiyama K, Yamaji M, Fujii M, Yamamoto T, Horie M (2010) Prognostic role of highly sensitive cardiac troponin I in patients with systolic heart failure. Am Heart J 159:63–67

Vasan RS, Levy D (1996) The role of hypertension in the pathogenesis of heart failure. A clinical mechanistic overview. Arch Intern Med 156:1789–1796

Yeh ET, Bickford CL (2009) Cardiovascular complications of cancer therapy: incidence, pathogenesis, diagnosis, and management. J Am Coll Cardiol 53:2231–2247

doi:10.1186/2193-1801-3-620
Cite this article as: Katsurada *et al.*: High-sensitivity troponin T as a marker to predict cardiotoxicity in breast cancer patients with adjuvant trastuzumab therapy. *SpringerPlus* 2014 3:620

HORM CANC (2014) 5:414–423
DOI 10.1007/s12672-014-0199-5

ORIGINAL PAPER

RhoC Upregulation Is Correlated with Reduced E-cadherin in Human Breast Cancer Specimens After Chemotherapy and in Human Breast Cancer MCF-7 Cells

Hirotoshi Kawata · Tomoko Kamiakito · Yawara Omoto · Chieko Miyazaki · Yasuo Hozumi · Akira Tanaka

Received: 5 June 2014 / Accepted: 28 July 2014 / Published online: 15 August 2014

Abstract Therapy-resistant cancer cells are a major problem in cancer research. Recent studies suggest that the epithelial-mesenchymal transition (EMT) is a key mechanism in therapy resistance. Yet, the expressions of EMT markers, EMT core regulators, and a stem cell marker of BMI1 during chemotherapy have been poorly analyzed in clinical breast cancer specimens. In the present study, we investigated the roles of RhoC under chemotherapy to follow up on earlier findings demonstrating the involvement of RhoC in prostate cancer resistance to endocrine therapy. Immunohistochemically, E-cadherin expression was significantly lower in human breast cancer specimens analyzed after chemotherapy than specimens biopsied before chemotherapy. Significant upregulation of fibronectin, a mesenchymal EMT marker, was found in post-chemotherapy analysis. A study of the EMT core regulators of SNAIL1, SNAIL2, TWIST1, and a well-known stem cell marker of BMI1 revealed no post-chemotherapy upregulation of these molecules. In contrast, RhoC expression was significantly upregulated in post-chemotherapy breast cancer specimens. MCF-7 cells stably transfected with the constitutive active (CA) RhoC plasmid manifested a reduced level of E-cadherin at the peripheries and disorganization of actin fibers, with no accompanying upregulation of SNAIL1, SNAIL2, TWIST1, or BMI1 in Western blots. Exposure of etoposide on MCF-7 cells showed RhoC upregulation together with reduced membranous expression of E-cadherin and disorganization of actin fibers. In MTT assay, however, the CA-RhoC-expressing MCF-7 cells failed to show chemotherapy resistance under etoposide treatment. Taken in sum, RhoC may contribute to an EMT-like process in human breast cancer during chemotherapy.

Electronic supplementary material The online version of this article (doi:10.1007/s12672-014-0199-5) contains supplementary material, which is available to authorized users.

H. Kawata · T. Kamiakito · A. Tanaka (✉)
Department of Pathology, Jichi Medical University, 3311-1 Yakushiji, Shimotsuke, Tochigi 329-0498, Japan
e-mail: atanaka@jichi.ac.jp

Y. Omoto · C. Miyazaki · Y. Hozumi
Breast Surgery, Jichi Medical University, Shimotsuke, Tochigi 329-0498, Japan

Introduction

Breast cancer is the leading cause of cancer death in women worldwide. Recent advances in molecular biology allow us to draw a clear landscape of the molecular networks in breast cancer [1]. Highly effective drugs are being continuously developed based on this information [2]. Yet, novel therapeutic approaches are still clearly needed, as tumors tend to relapse after undergoing existing therapies of various types. Recent studies have revealed that the epithelial-mesenchymal transition (EMT) takes part in chemotherapy and endocrine therapy resistance in breast cancer [3–5]. The EMT is also shown to be involved in the generation of cancer stem cells (CSCs) [6], a class of cells believed to be highly therapy resistant [7]. Further, the CSC-related molecule BMI1 has been shown to both contribute to chemotherapy resistance [8] and induce the EMT [9]. These findings, taken together, suggest that the EMT and CSCs are strongly linked to chemotherapy resistance. The EMT was originally described as a loss of E-cadherin and gain of mesenchymal markers in cancer cells, a process that mimicked mesoderm and neural crest formation during embryogenesis [10, 11]. The Snail and Twist homologs are defined as core transcriptional repressors that directly bind to the E-cadherin promoter [10, 11]. While several immunohistochemical analyses have focused on the expressions of BMI1 and the Snail and Twist homologs in human breast cancer [12, 13], none before now have

compared these molecules in human breast cancer specimens of the same patient before and after chemotherapy.

We have recently shown that RhoC is linked to cancer cell survival through a partial epithelial-mesenchymal transition (EMT) process after endocrine therapy in cultured mouse breast cancer cells and human prostate cancer specimens [14]. The Rho small GTPases are major regulators of actin dynamics and play a role in cell motility [15]. The Rho GTPases are subdivided into three subfamilies respectively descended from the prototypal proteins RhoA, Rac1, and Cdc42 [16]. The activation of RhoA, RhoB, and RhoC, the three highly homologous isoforms of the RhoA family, facilitates amoeboid cell movement by stimulating the organization of actin stress fibers (ASFs) [15, 16]. Among the three isoforms, RhoC was found to play a key role in tumor progression [17–20]. Two earlier studies on human breast cancer have shown a correlation between RhoC expression and aggressive phenotypes [21, 22]. Little is known, however, about the roles of RhoC in human breast cancer during chemotherapy.

In the present comparison of human breast cancer specimens between pre- and post-chemotherapy, the upregulation of RhoC and the downregulation of E-cadherin were both significantly increased after the chemotherapy. In contrast, we found no significant upregulation of SNAIL1, SNAIL2, TWIST1, or BMI1. Lastly, transfection of the constitutive active (CA) RhoC plasmid into human breast cancer MCF-7 cells reduced the membranous localization of E-cadherin. These findings implicate RhoC as a key factor in breast cancer progression under chemotherapy.

Materials and Methods

Cases

Tumor specimens from 50 breast cancer cases resected after chemotherapy were retrieved from the archives of the Pathology Department of Jichi Medical University Hospital. All cases, diagnosed as invasive ductal carcinomas, had undergone core needle biopsy before chemotherapy, and each biopsied specimen was compared to the resected specimen from the same patient. The patient characteristics are summarized in Table 1 and shown in detail in Supplementary Table S1. The chemotherapy protocols, which varied considerably from case to case, are also shown in Supplementary Table S1. Data on the estrogen receptor (ER), progesterone receptor (PgR), and Her2 were retrieved from the clinical records. The duration of chemotherapy was 63 to 504 days (mean 152 days). Immunohistochemical studies were performed with the approval of the local ethics committee at Jichi Medical University.

Table 1 Characteristics of the patients

Cases (n=50)		
Age (years)		52.5 (32~85)
Menopause		27
Clinical stage	IIA	20
	IIB	13
	IIIA	3
	IIIB	9
	IIIC	5
Tumor size (mm)		32.7 (14~80)
Duration of primary systemic therapy (PST) (days)		152 (63~504)
Interval between PST and operation (days)		29 (1~214)

Cells

Estrogen-sensitive human breast cancer MCF-7 cells were maintained in a DMEM medium supplemented with 10 % fetal bovine serum (FBS) in the presence of insulin (4 μg/ml) and 17β-estradiol (E2) (100 nM).

Plasmids, Mutagenesis, and Isolation of Stable Transfectant Cells

The method for constructing the mouse constitutive active (CA) RhoC (G12V) expression plasmid was described previously [14]. MCF-7 cells were transfected with the CA-RhoC plasmid by a Lipofectamin (Invitrogen, Carlsbad, CA) method and then selected using 800 μg/ml of G418 sulfate (GIBCO/Invitrogen). Two clones with standard expression of the tagged protein in Western blots were used in further experiments.

Immunohistochemistry and Antibodies

Supplementary Table S2 summarizes the antibodies used in this study and the methods for antigen retrieval and detection. In general, formalin-fixed and paraffin-embedded sections were pre-treated in a microwave oven or an autoclave for the indicated times. Next, the sections were allowed to interact with each antibody at 4 °C overnight, subjected to either standard treatment with avidin-biotin complex or incubation with Envision (DAKO JAPAN, Tokyo, Japan), and stained with DAB. The immunostaining was scored as follows according to the criteria previously reported by our group [14]: (−), negative; (±), weakly positive in less than 20 % of cancer cells; (+), distinctly positive in 20 to 80 % of cancer cells; and (++), strongly positive in more than 80 % of cancer cells.

Rho Activation Assay

An Rho activation assay was performed using the Rho Activation Assay Kit (Upstate/MILLIPORE, Temecula, CA) by the method described in our earlier report [14]. Briefly, cell extracts were prepared by incubation for 48 h in a DMEM medium containing 10 % FBS in the presence of E2 and insulin. The extracted proteins were incubated with Rhotekin Rho-binding domain agarose beads for 45 min at 4 °C with gentle agitation. The beads were washed three times with the buffer provided, and then the pellets were resolved by a standard sodium dodecyl sulfate polyacrylamide gel electrophoresis (SDS-PAGE) and transferred to the polyvinylidene difluoride (PVDF) membrane. The blots were incubated with the Rho antibody provided in the kit and then detected with an ECL prime kit (GE Healthcare, Buckinghamshire, UK).

Western Blots

Cell extracts were prepared in the DMEM-maintained medium in a sub-confluent condition with a cell lysis reagent of CelLytic M (Sigma-Aldrich, St. Louis, MO). In the study of RhoC expression under etoposide treatment, MCF-7 cells (1.2×10^6/dish) were plated in a phenol-red-free RPMI 1640 medium supplemented with 2 % FBS treated with dextran-coated charcoal (dcc) in the absence of E2 and insulin. The

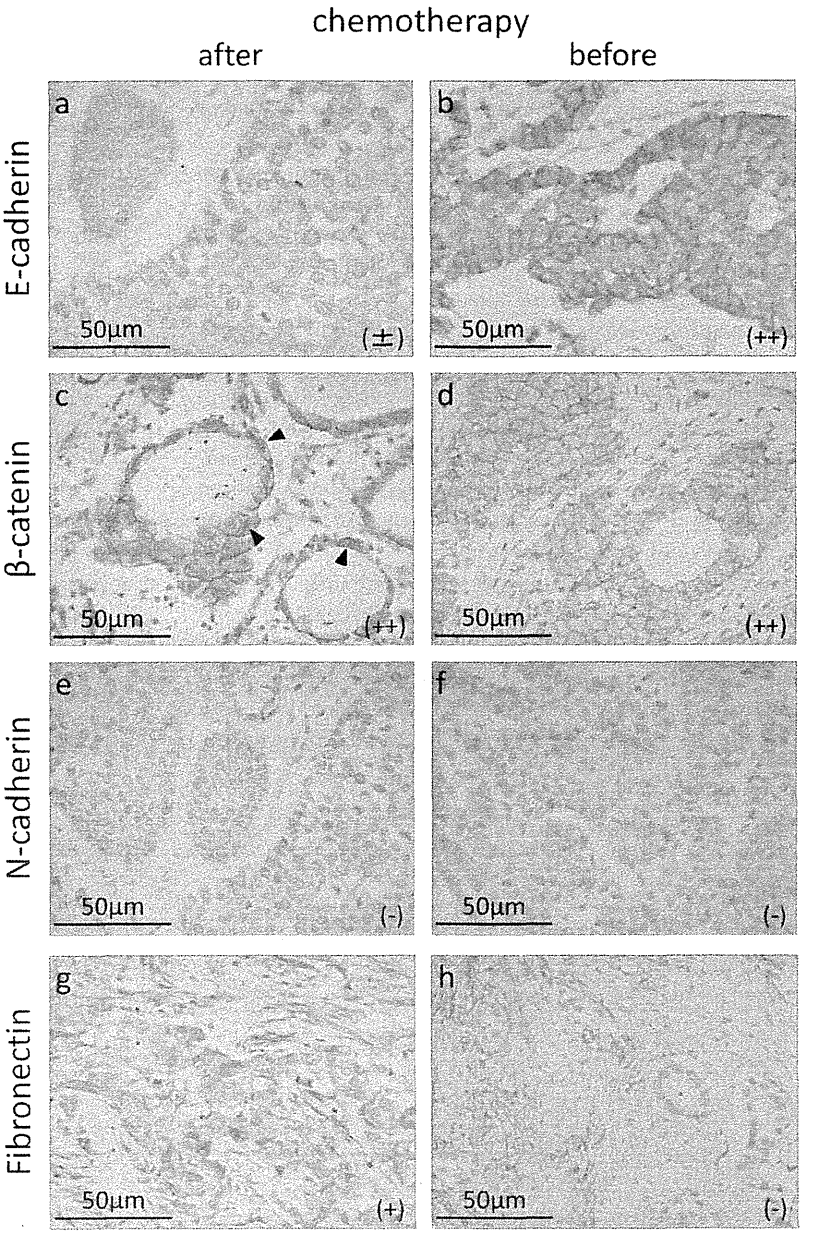

Fig. 1 Immunohistochemical comparison of E-cadherin, β-catenin, N-cadherin, and fibronectin between pre- and post-chemotherapy of the same case in human breast carcinoma specimens. Immunostaining of E-cadherin (**a**, **b**), β-catenin (**c**, **d**), N-cadherin (**e**, **f**), and fibronectin (**g**, **h**) in human breast cancer specimens surgically resected after chemotherapy (*after*) (**a**, **c**, **e**, **g**) and in biopsied specimen of the same case before chemotherapy (*before*) (**b**, **d**, **f**, **h**). The *arrowhead* indicates nuclear translocation of β-catenin in one case (**d**). The immunohistochemical scoring is also shown as (−), (±), (+), and (++)

cells were further cultured for 5 days in a phenol-red-free RPMI 1640 medium containing 2 % dcc-treated FBS in the absence or presence of 100 nM E2 and/or 10 μM of etoposide (Wako Pure Chemical Industries, Osaka, Japan), with medium changes every other days. Cell extracts were similarly prepared. In general, 20 μg of lysates was separated by SDS-PAGE electrophoresis and transferred onto PVDF membranes. The blots were reacted with the antibodies listed in Supplementary Table S2, and the signals were detected with an ECL prime kit. For loading controls, the membranes were stripped with reprobe buffer [62.5 mM Tris–HCl (pH 6.8), 100 mM 2-mercaptoethanol, 2 % SDS] at 60 °C for 30 min and then immunoblotted with an anti-GAPDH antibody (MILLIPORE, Temecula, CA) followed by the secondary antibody.

Phalloidin Staining and Immunocytochemistry of E-cadherin

The method for phalloidin staining was described previously [14]. Briefly, MCF-7 cells (1.2×10^4/well) were plated onto a 4-well chamber slide. The next day, the medium was changed to the DMEM-maintained medium. After a 6 h culture, the cells were fixed in a PBS solution with 4 % paraformaldehyde for 60 min, treated with 0.1 % Triton-X for 5 min, and stained with rhodamine-labeled phalloidin. The specimens were observed with a fluorescence microscope. In the study of etoposide treatment, cells were plated and culture onto a 4-well chamber slide using a phenol-red-free RPMI1640 medium containing 2 % dcc FBS in the absence or presence of E2 and/or etoposide. After culture for 5 days, cells were similarly fixed and stained with rhodamine-labeled phalloidin. In immunocytochemistry of E-cadherin, cells were similarly cultured, fixed, incubated with the anti-E-cadherin antibody, and then reacted with a fluorescein isothiocyanate (FITC)-conjugated secondary antibody. The slide was observed with a fluorescence microsocpe.

MTT Assay

Parental and transfectant MCF-7 cells (6.0×10^3/well) were plated onto a 96-well plate in a phenol-red-free RPMI 1640 medium supplemented with 2 % dcc-treated FBS in the absence of insulin and E2. The next day (day 1), the medium was changed to the phenol-red-free RPMI 1640 medium with 2 % dcc-treated FBS in the presence or absence of E2 and/or 10 μM of etoposide. The medium was changed once on day 3, and MTT was added to the medium at a final concentration of 1 mg/ml on day 5. After 4 h of incubation with the MTT, formazan substrates were collected, resolved with DMSO, and measured at an absorbance of 570 nm, with reference at 690 nm.

Statistical Analysis

The statistical significance of value changes was determined by the Wilcoxon signed-ranks test or Mann-Whitney's *U* test using Statcel software (OMS, Saitama, Japan). Results were considered significant when the *P* values were less than 0.05.

Results

Membranous E-cadherin localization is reduced after chemotherapy in human breast cancer

To confirm the involvement of the EMT process in chemotherapy resistance, we began our experiment by comparing E-cadherin expression in cancer specimens biopsied before surgery with specimens surgically resected after chemotherapy. In spite of considerable variation in the chemotherapy protocols from case to case, E-cadherin expression was significantly more downregulated after chemotherapy compared to before ($P<0.0002$) (Fig. 1a, b and Table 2). Next, we sought to

Table 2 Immunohistochemical results

($n = 50$)

	E-cadherin		β-catenin		N-cadherin		Fibronectin	
	after	before	after	before	after	before	after	before
(++)	30	47	36	40	1	1	0	0
(+)	17	2	13	9	2	0	34	3
(±)	3	1	0	0	13	13	15	18
(-)	0	0	1	1	34	36	1	29
	$P<0.0002$		$P=0.248$		$P=0.317$		$P<0.0001$	

determine whether any enhancement of the nuclear translocation of β-catenin accompanied the reduction of E-cadherin. β-catenin expression in cytoplasmic membranes was unchanged after chemotherapy (P=0.248), and the nuclear translocation of β-catenin was almost undetectable in all but one post-chemotherapy specimen (Fig. 1c, d and Table 2). On examination of mesenchymal markers, significant upregulation was found in fibronectin, but not in N-cadherin, between pre- and post-chemotherapy (P<0.0001 and P=0.317) (Fig. 1e–h and Table 2). The induction of a partial EMT seems very likely after breast cancer chemotherapy, given the great importance of the membranous expression of E-cadherin as a factor in epithelial phenotypes.

Neither SNAIL1, SNAIL2, TWIST1, nor BMI1 expression was upregulated after chemotherapy in human breast cancer.

Next, we compared the expressions of SNAIL1, SNAIL2, TWIST1, and BMI1 between pre- and post-chemotherapy. The nuclear expressions of SNAIL1, SNAIL2, and TWIST1 were shown to be significantly downregulated, not upregulated, after chemotherapy (P<0.05) (Fig. 2a–f and Table 3). We also observed a significant downregulation of BMI1 expression after chemotherapy (P<0.05) (Fig. 2g, h and Table 3). These findings suggest that SNAIL1, SNAIL2, TWIST1, and BMI1 are less likely to be involved in the partial EMT under chemotherapy in human breast cancer.

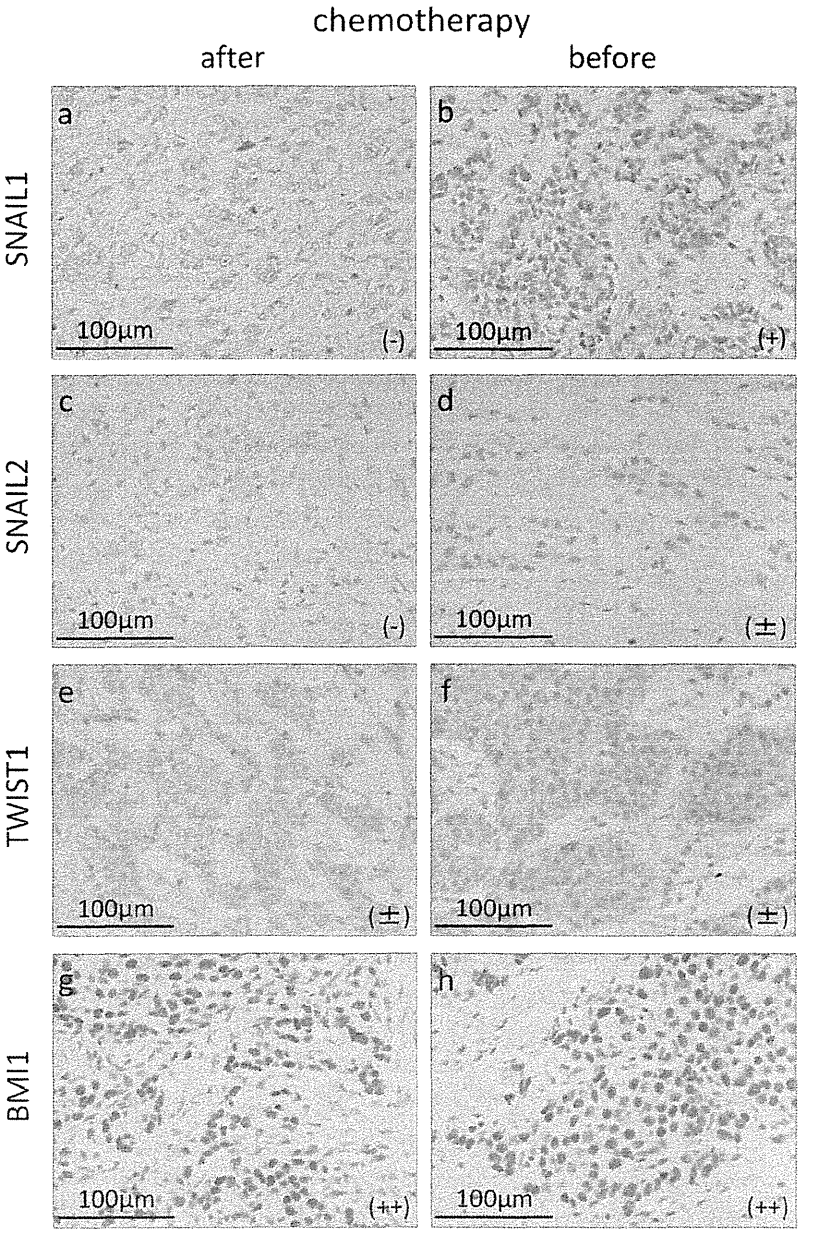

Fig. 2 Immunohistochemical comparison of SNAIL1, SNAIL2, TWIST1, and BMI1 between pre- and post-chemotherapy of the same case in human breast carcinoma specimens. Immunostaining of SNAIL1 (**a**, **b**), SNAIL2 (**c**, **d**), TWIST1 (**e**, **f**), and BMI1 (**g**, **h**) in human breast cancer specimens surgically resected after chemotherapy (*after*) (**a**, **c**, **e**, **g**) and in biopsied specimen of the same case before chemotherapy (*before*) (**b**, **d**, **f**, **h**). The immunohistochemical scoring is also shown

Table 3 Immunohistochemical results

($n = 50$)

	SNAIL1		SNAIL2		TWIST1		BMI1		RhoC		NET1	
	after	before	after	before	after	before	after	before	after	before	after	before
(++)	2	0	1	0	0	0	41	48	45	29	0	6
(+)	6	26	0	7	2	0	7	2	5	21	11	30
(±)	13	33	3	6	28	48	2	0	0	0	17	8
(-)	29	1	46	37	20	2	0	0	0	0	22	6
	$P < 0.0001$		$P < 0.05$		$P < 0.0005$		$P < 0.05$		$P < 0.0002$		$P < 0.0001$	

RhoC is expressed at a higher level after chemotherapy than before in human breast cancer.

Rho small GTPases are well established to play a key role in cytoskeletal actin dynamics involved in the regulation of cadherin-mediated cell-cell adhesion. Our earlier data on the involvement of RhoC in endocrine therapy resistance in prostate cancer [14] prompted us to compare the expressions of RhoC and NET1 (a Rho-specific guanine exchange factor) in human breast cancer specimens between pre- and post-chemotherapy. RhoC expression was significantly more upregulated in the specimens resected after chemotherapy than in the specimens biopsied before the therapy ($P<0.0002$) (Fig. 3a, b and Table 3). In contrast to our earlier finding in prostate cancer [14], the expression of NET1 was significantly downregulated after the therapy ($P<0.0001$) (Fig. 3c, d and Table 3). This alteration in RhoC expression suggests that other Rho guanine nucleotide exchange factors may be involved in RhoC activation in breast cancer. The findings also suggest that RhoC activation has the potential to reduce the membranous expression of E-cadherin, possibly by regulating actin dynamics, under human breast cancer chemotherapy.

Stable transfection with a CA-RhoC plasmid into MCF-7 cells reduces membranous E-cadherin expression and disrupts the organization of actin fibers.

We next investigated whether or not stable transfection of a CA-RhoC expression plasmid into MCF-7 cells induces an EMT process. An Rho activation assay (Fig. 4a) confirmed the function of the transfected gene by revealing higher Rho activity in MCF-7 cells expressing CA-RhoC than in parental MCF-7 cells. In immunocytochemistry and phalloidin staining, the CA-RhoC-expressing cells exhibited reduced E-cadherin expression at the peripheries of the cancer cell nests and disorganized actin fibers (Fig. 4c, d, f, g). In contrast, no

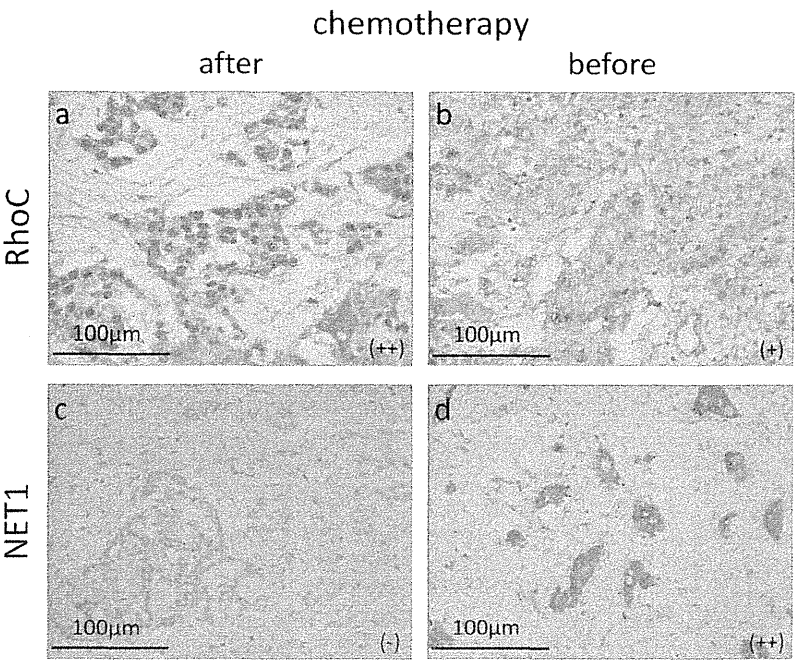

Fig. 3 Immunohistochemical comparison of RhoC and NET1 between pre- and post-chemotherapy in human breast carcinoma specimens. RhoC (**a**, **b**) and NET1 (**c**, **d**) immunostaining in a breast cancer specimen surgically resected after chemotherapy (*after*) (**a**, **c**) and in the biopsied specimen of the same case before chemotherapy (*before*) (**b**, **d**). The immunohistochemical scoring is also shown

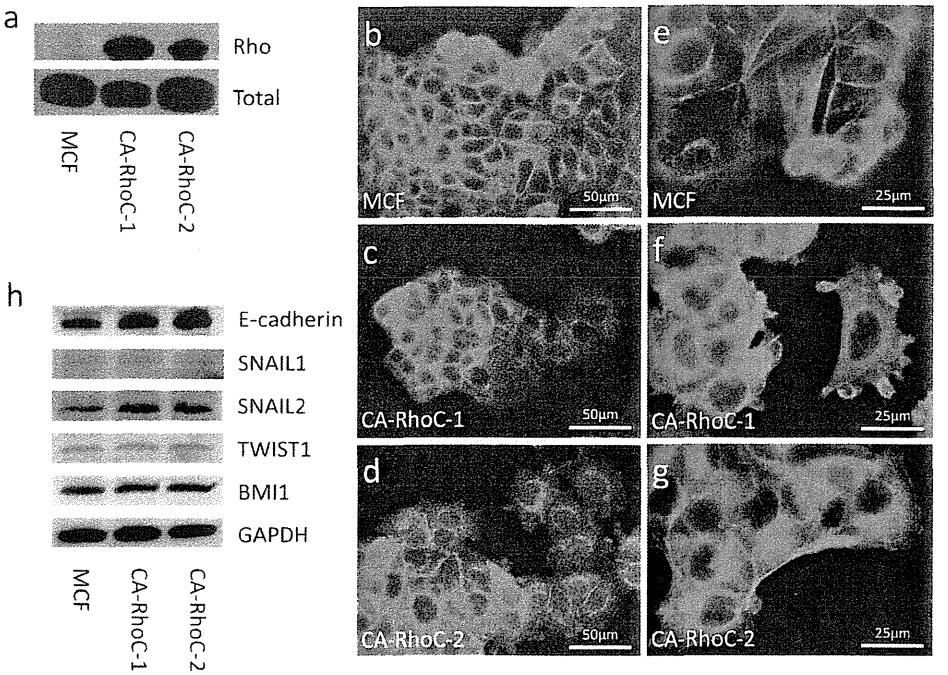

Fig. 4 Reduction of E-cadherin and disorganization of actin fibers in CA-RhoC-expressing MCF-7 cells. Rho activation assay in transfectant and parental MCF-7 cells (**a**). Cell extracts were prepared from subconfluent CA-RhoC-expressing MCF-7 cells and parental MCF-7 cells with the lysate solution in the kit. Four hundred micrograms of extracted protein was incubated with Rhotekin Rho-binding domain agarose beads. The pellets were analyzed by Western blots using the Rho antibody provided in the kit (Rho). The total levels of RhoA family GTPases (*Total*), namely, RhoA, RhoB, and RhoC, are shown at the *bottom*. Immunocytochemistry of E-cadherin (**b**, **c**, **d**). Transfectant (CA-RhoC-1, -2) and parental (MCF) MCF-7 cells (1.2×10^4/well) were plated onto a 4-well chamber slide. The medium was exchanged once on the next day and cultured for 6 h. The cells were fixed with 4 % paraformaldehyde, incubated with the anti-E-cadherin antibody, and reacted with an FITC-conjugated secondary antibody. The slide was observed with a fluorescence microscope. Phalloidin staining (**e**, **f**, **g**). Transfectant (CA-RhoC-1, -2) and parental (MCF) MCF-7 cells were similarly plated and cultured onto a 4-well chamber slide. The cells were fixed with 4 % paraformaldehyde, stained with rhodamine-labeled phalloidin, and observed with a fluorescence microscope. Western blots (**h**). Cell lysates were prepared from subconfluent CA-RhoC-expressing MCF-7 cells and the parental MCF-7 cells with the lysis solution indicated in the Materials and Methods section. The cell lysates (20 μg) were separated by SDS-PAGE electrophoresis and transferred onto PVDF membranes. The blots were reacted with the antibodies of E-cadherin, SNAIL1, SNAIL2, TWIST1, and BMI1. Signals were detected with an ECL prime kit. The *bottom panel* shows the loading controls of GAPDH

signs of E-cadherin loss or actin fiber disorganization were observed in the parental MCF-7 cells (Fig. 4b, e). In Western blots using whole cell lysates, the overall E-cadherin levels were comparable in the transfectant and parental cells (Fig. 4h), suggesting that membranous E-cadherin expression is disorganized in the CA-RhoC-expressing cells. Nuclear localization of β-catenin was undetectable in CA-RhoC-expressing MCF-7 cells (data not shown). No significant upregulation of SNAIL1, SNAIL2, TWIST1, or BMI1 was found in CA-RhoC-expressing MCF-7 cells versus the parental cells in Western blots (Fig. 4h). These observations suggest that RhoC is one of the regulatory factors involved in the reduction of the membranous localization of E-cadherin.

Rho activity is not directly linked with resistance to etoposide treatment in CA-RhoC-expressing MCF-7 cells.

We next analyzed effects of etoposide treatment on the EMT process and RhoC expression in MCF-7 cells. RhoC expression is elevated under etoposide treatment in the presence of E2 in MCF-7 cells (Fig. 5a). Although overall levels of E-cadherin expression were unchanged (Fig. 5a), immunocytochemistry displayed that membranous E-cadherin expression is reduced at the peripheries of cancer cell nests under etoposide treatment together with disorganization of actin fibers (Fig. 5b–i). Upon exposure to etoposide in the presence of E2, the cell viability of CA-RhoC-expressing MCF-7 cells was reduced to 49.8 and 51.4 %, levels similar to that observed in the parental cells (48.8 %) (Fig. 5j, k). In the absence of E2, the treatment with etoposide mildly lowered the cell viability to 94.2 % ($P<0.05$) and 73.7 % ($P=0.275$) in the transfectant cells, versus 67.9 % in the parental cells (Fig. 5j, k). In view of apoptosis, cleaved caspase 3, a well-known apoptotic marker, was faintly detected only in the parental MCF-7 cells in the presence of E2 (Supplementary Fig. S1). In TUNEL assay, labeled cells were at marginal levels in the parental and the trasfectant MCF-7 cells (data not shown). Both findings suggest that involvement